The Effects of Surface Elasticity on an Elastic Solid With Mode-III Crack: Complete Solution

C. I. Kim

P. Schiavone[1]
e-mail: p.schiavone@ualberta.ca

C.-Q. Ru

Department of Mechanical Engineering,
University of Alberta,
Edmonton,
AB, T6G 2G8, Canada

We examined the effects of surface elasticity in a classical mode-III crack problem arising in the antiplane shear deformations of a linearly elastic solid. The surface mechanics are incorporated using the continuum based surface/interface model of Gurtin and Murdoch. Complex variable methods are used to obtain an exact solution valid everywhere in the domain of interest (including at the crack tip) by reducing the problem to a Cauchy singular integro-differential equation of the first order. Finally, we adapt classical collocation methods to obtain numerical solutions, which demonstrate several interesting phenomena in the case when the solid incorporates a traction-free crack face and is subjected to uniform remote loading. In particular, we note that, in contrast to the classical result from linear elastic fracture mechanics, the stresses at the (sharp) crack tip remain finite. [DOI: 10.1115/1.3177000]

Keywords: surface elasticity, mode-III crack, antiplane deformations, complete exact solution, Cauchy singular integro-differential equation

1 Introduction

Currently, the two fundamental approaches used in the modeling of the deformation of solids at the nanoscale involve either atomistic models or refined continuum models. The former rely on massive atomistic simulations, which most often require huge computational resources. Nonetheless, these models were used successfully to investigate problems of great interest in nanomechanics including several problems involving fracture and related issues (see, for example, Refs. [1–4]). Refined continuum models offer the advantages of the continuum setting and the associated mathematical framework. This "refinement" of classical continuum theories to account for the nanoscale is most often achieved by incorporating the effects of surface mechanics on the structural boundaries of the solid in an attempt to account for the increasing surface area to volume ratio of structures at this scale. Experiments on various elastic structures (e.g., beams, plates, and shells) showed that predictions from these continuum models had good agreement with corresponding results obtained from the atomistic simulations (see, for example, Refs. [5,6]). One of the most important and accessible refined continuum models incorporates the effects of surface mechanics using the surface elasticity model of Gurtin and co-workers [7,8]. In this model, a surface is regarded as a thin elastic membrane perfectly bonded to the bulk solid. The additional surface stress contributed by the surface mechanics leads to highly unusual and nonstandard boundary conditions on the surface of the bulk solid. Consequently, the corresponding boundary value problems are not accommodated by existing classical theories and pose challenges not encountered previously in similar mathematical analyses. Nonetheless, the Gurtin and Murdoch assumptions were used successfully in a number of studies, for example, in nanocomposite mechanics (see, for example, Refs. [5,9–12]).

The analysis of stresses in an elastic solid incorporating one or more cracks is of fundamental importance in the understanding of failure and in the general deformation analysis of engineering materials. In macroscopic models, the stresses at the crack tip are found to be infinite reflecting the fact that the crack front is usually taken to be perfectly sharp. In fact, an infinitely sharp crack in a continuum is a mathematical abstraction since, in reality, most crack tips are, in fact, blunt with a radius of convergence of the order compatible with the nanoscale. This suggests that a more accurate analysis of the region in the vicinity of a crack tip can be achieved at the nanoscale. In the context of a continuum model this means the incorporation of surface effects into the model of deformation. In fact, it was shown using atomistic models that the influence of surface energy is significant in the vicinity of the crack tip [13]. To this end, the authors in Ref. [14] examined the contribution of surface effects on the near-tip stresses of a mode-III crack using the Gurtin–Murdoch theory under several simplifying assumptions including the assumption that the crack tip is blunt with a radius of convergence of the order compatible with the nanoscale. Approximate numerical results are presented using asymptotic and finite element methods. These results, however, are restricted to the vicinity of the crack tip and do not present a complete solution of the problem at hand. The authors also note the contributions made in Refs. [15–18] in which the effects of surface stresses were considered in a range of different problems involving elastic solids. In each case, however, the results in Refs. [15–18] employed simplified assumptions on the stress-strain relations used to model the effects of surface elasticity. In particular, the surface stress is taken to be independent of surface strain. This assumption, although leading to simplified and thus tractable mathematical models of the corresponding solid, sacrifice the rigor and accuracy of a more comprehensive theory.

In this paper we present an exact complete (valid throughout the domain of interest and not simply in the vicinity of the crack tip) solution of a traction-free mode-III crack problem in the antiplane shear deformations of a linearly elastic solid maintaining the assumption of a sharp crack tip. Surface effects are incorporated using the Gurtin–Murdoch surface elasticity model (with complete constitutive relations on the surface of the solid) with the crack occupying a finite region of the real axis. Using complex variable techniques, we show that the nonstandard boundary conditions arising from the incorporation of the effects of surface elasticity on the crack face were reduced to the solution of a Cauchy singular integro-differential equation [19]. The latter is solved numerically using an adapted collocation technique [20]

[1]Corresponding author.

Contributed by the Applied Mechanics Division of ASME for publication in the JOURNAL OF APPLIED MECHANICS. Manuscript received January 9, 2009; final manuscript received May 31, 2009; published online December 11, 2009. Review conducted by Zhigang Suo.

leading to a complete solution throughout the elastic solid. In particular, it is shown that, in contrast to classical fracture mechanics (where surface effects are neglected), the incorporation of surface elasticity eliminates the stress singularity at the (infinitely sharp) crack tip and leads to the more accurate situation of a finite stress at the crack tip. In addition, we demonstrate that the corresponding stress distributions derived from our analysis show clear signs of size dependency and do indeed tend to classical solutions [21,22] when the surface effects approach zero.

Throughout the paper, we make use of a number of well-established symbols and conventions. Thus, unless otherwise stated, Greek and Latin subscripts take the values 1,3 and 1,2,3, respectively, summation over repeated subscripts is understood, (x,y) and (x,y,z) are generic points referred to orthogonal Cartesian coordinates in $\mathbb{R}^2$ and $\mathbb{R}^3$, respectively, and δ_{ij} is the Kronecker delta.

2 Antiplane Crack Problem With Surface Stress: Governing Equations

It is well-known that in the absence of body forces, the equilibrium and constitutive equations describing the deformation of a linearly elastic, homogeneous, and isotropic (bulk) solids are given by

$$\text{div } \sigma^B = 0 \tag{1a}$$

$$\sigma^B = \lambda \boldsymbol{I}_3 \, Tr(\varepsilon) + 2\mu\varepsilon \tag{1b}$$

where λ and μ are the Lame constants of the material; σ^B and ε are the stress and strain tensors, respectively; and $\boldsymbol{I}_3$ represents the identity tensor with respect to $\mathbb{R}^3$.

2.1 Surface Equation. We consider antiplane deformations of a linearly elastic and homogeneous isotropic solid occupying a cylindrical region in $\mathbb{R}^3$ with generators parallel to the z-axis of a rectangular Cartesian coordinate system. We assume that the cylinder is infinite in extent and is subjected to uniform remote shear stress. Suppose that the cylinder contains a single internal crack face (with traction-free faces) running the length of the cylinder. In a typical cross section, the crack occupies the region $[-a,a]$, $a \in \mathbb{R}^+$ of the x-axis as shown in Fig. 1. The objective here is to incorporate the surface mechanics of the crack face into the model describing the antiplane deformations of the solid. In the Gurtin–Murdoch surface elasticity model, the authors regard a surface as a thin elastic membrane (with elastic constants distinct from the bulk material) perfectly bonded to the surrounding material. Although Eqs. (1*a*) and (1*b*) remain true in the bulk material, equilibrium on the (crack) surface is now described by the equations (see Refs. [7,8] for detailed derivations)

$$[\sigma^B \boldsymbol{n}] + \text{div}_s \, \sigma^s = 0 \tag{2a}$$

$$\sigma^s = \sigma_o \boldsymbol{I}_2 + 2(\mu^s - \sigma_o)\boldsymbol{\varepsilon}^s + (\lambda^s + \sigma_o) Tr(\boldsymbol{\varepsilon}^s)\boldsymbol{I}_2 \tag{2b}$$

Here, the index s denotes the corresponding quantity resulting from the effects of surface elasticity, $\boldsymbol{n}$ represents the unit normal to the crack face, $\boldsymbol{I}_2$ is the identity tensor in $\mathbb{R}^2$, $[*]=(*)^+-(*)^-$ denotes the jump of the corresponding quantity across the crack (here "+" and "−" refer, respectively, to the upper face $(y>0)$ and lower face $(y<0)$ of the crack as depicted in Fig. 1), and σ_o is the surface tension. We note that only surface strain components are included in Eq. (2*b*) (i.e., strains normal to the surface are excluded). Finally, the surface divergence $\text{div}_s \boldsymbol{u}$ is defined (in general) by

$$\text{div}_s \boldsymbol{u} = \text{div}_s \boldsymbol{u}_s - 2\bar{k} u_n$$

where $\bar{k}$ is the mean curvature and the displacement vector $\boldsymbol{u}$ admits the unique decomposition as follows:

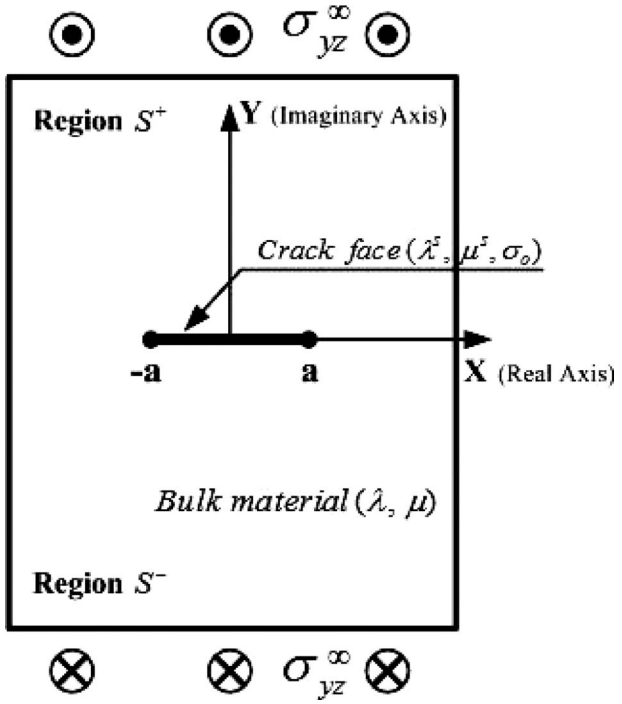

Fig. 1 Schematic of the problem

$$\boldsymbol{u} = \boldsymbol{u}_s + u_n \boldsymbol{n}$$

with $\boldsymbol{u}_s$ as the corresponding tangential displacement and u_n as the normal component of $\boldsymbol{u}$.

2.2 Complex-Variable Formulation. Equation (1*b*) is written in component form as

$$\sigma_{ij} = \lambda \delta_{ij}\varepsilon_{kk} + \mu\varepsilon_{ij} \tag{3a}$$

$$\varepsilon_{ij} = \tfrac{1}{2}(u_{i,j} + u_{j,i}) \tag{3b}$$

In the antiplane shear of an isotropic elastic medium (mode-III crack problem), we assume that the displacement vector $\boldsymbol{u}$ with components (u,v,w) satisfies

$$u = v = 0, \quad w = w(x,y), \quad \frac{\partial^2 w}{\partial x^2} + \frac{\partial^2 w}{\partial y^2} = 0 \tag{4}$$

From Eq. (3*b*), the strain components are now given by

$$\varepsilon_{xz} = \frac{1}{2}\left(\frac{\partial u}{\partial z} + \frac{\partial w}{\partial x}\right) = \frac{1}{2}\frac{\partial w}{\partial x}, \quad \varepsilon_{yz} = \frac{1}{2}\left(\frac{\partial v}{\partial z} + \frac{\partial w}{\partial y}\right) = \frac{1}{2}\frac{\partial w}{\partial y}$$

$$\varepsilon_{xy} = \varepsilon_{xx} = \varepsilon_{yy} = \varepsilon_{zz} = 0 \tag{5}$$

From Eq. (5), the stress components can be written as

$$\sigma_{xz} = 2\mu\varepsilon_{xz} = \mu\frac{\partial w}{\partial x}, \quad \sigma_{yz} = 2\mu\varepsilon_{yz} = \mu\frac{\partial w}{\partial y}$$

$$\sigma_{xy} = \sigma_{xx} = \sigma_{yy} = \sigma_{zz} = 0 \tag{6}$$

Since $w(x,y)$ is a harmonic function, we denote by $\psi(x,y)$ its conjugate harmonic function. Introducing the complex variable $z = x+iy$, we can now write

$$w = \text{Re}[\Omega(z)], \quad \Omega(z) = w(x,y) + i\psi(x,y) \tag{7}$$

where $\Omega(z)$ is an analytic function of z in the plane $S^+ \cup S^- = S$ outside the crack (see Fig. 1). From Eq. (7), we then have that

$$\frac{d\Omega}{dz}(z) = \Omega'(z) = \frac{\partial w}{\partial x} - i\frac{\partial w}{\partial y} = \frac{1}{\mu}(\sigma_{xz} - i\sigma_{yz}) \tag{8}$$

and

$$\sigma_{yz} = \frac{\mu i}{2}[\Omega'(z) - \overline{\Omega'(z)}], \quad \sigma_{xz} = \frac{\mu}{2}[\Omega'(z) + \overline{\Omega'(z)}] \tag{9}$$

2.3 Equilibrium Equations on the Crack Surface. If we denote by $\{\underline{e}_i\}_{i=1}^3$ the vectors of the standard basis for $\mathbb{R}^3$ from Eq. (2*a*), the equilibrium conditions on the crack surface are given by [7,8]

$$\begin{gathered}\sigma^s_{\alpha\beta,\beta}\underline{e}_\alpha + [\sigma_{ij}n_j\underline{e}_i] = 0 \\ k_{\alpha\beta}\sigma^s_{\alpha\beta} = [\sigma_{ij}n_in_j]\end{gathered} \tag{10}$$

where $\alpha,\beta=1,3$.

Noting that in our case the normal to the crack face is aligned with the $\underline{e}_2$ or y-direction, Eq. (10) becomes

$$\sigma^s_{xx,x} + \sigma^s_{xz,z} + [\sigma_{xy}] = 0 \tag{11a}$$

$$\sigma^s_{zx,x} + \sigma^s_{zz,z} + [\sigma_{yz}] = 0 \tag{11b}$$

$$[\sigma_{yy}] = -\sigma_o\frac{\partial^2\nu}{\partial x^2} - \sigma_o\frac{\partial^2\nu}{\partial z^2} \tag{11c}$$

In addition, we derive the component form of Eq. (2*b*) as

$$\sigma^s_{\alpha\beta} = \sigma_o\delta_{\alpha\beta} + 2(\mu^s - \sigma_o)\varepsilon_{\alpha\beta} + (\lambda^s + \sigma_o)\varepsilon_{\gamma\gamma}\delta_{\alpha\beta} \tag{12}$$

where $\alpha,\beta,\gamma=1,3$. Thus, together with Eqs. (5) and (6), we can now establish the relations between surface and body (bulk) stresses as

$$\begin{gathered}\sigma^s_{xz} = 2(\mu^s - \sigma_o)\varepsilon_{xz} = \frac{\mu^s - \sigma_o}{\mu}\sigma_{xz} \\ \sigma^s_{yz} = 2(\mu^s - \sigma_o)\varepsilon_{yz} = \frac{\mu^s - \sigma_o}{\mu}\sigma_{yz}\end{gathered} \tag{13}$$

since, for a coherent interface, the interfacial strains are equal to those in the adjoined bulk material, i.e., $\varepsilon^s_{xz}=\varepsilon_{xz}$ and $\varepsilon^s_{yz}=\varepsilon_{yz}$.

Finally, by applying the antiplane assumptions in Eqs. (5), (6), and (13), Eqs. (11*a*)–(11*c*) can be reduced to the form

$$\sigma^s_{xz,x} + [\sigma_{yz}] = 0 \tag{14}$$

2.4 A Traction-Free Mode-III Crack Problem With Surface Stress. Let the lower ($y<0$) and upper ($y>0$) half-planes be designated the "–" and "+" sides of the crack. Then, from Eq. (14), the boundary conditions on the crack can be written as

$$\frac{\partial\sigma^s_{xz}}{\partial x} + (\sigma_{yz})^+ - (\sigma_{yz})^- = 0 \tag{15}$$

In general, from Eqs. (5), (9), (13), and (15), for the crack $[-a \le x \le a]$, $(y=0)$ subjected to prescribed traction P_{yz}, the surface condition on the faces can be written as follows.

On the upper face,

$$\begin{aligned}(\sigma_{yz})^+ &= P_{yz} - \frac{\partial\sigma^s_{xz}}{\partial x} = P_{yz} - (\mu^s - \sigma_o)\frac{\partial^2 w}{\partial x^2} \\ &= P_{yz} - \frac{\mu^s - \sigma_o}{2}[\Omega''(z) + \overline{\Omega''(z)}]^+\end{aligned} \tag{16a}$$

On the lower face,

$$\begin{aligned}(\sigma_{yz})^- &= P_{yz} + \frac{\partial\sigma^s_{xz}}{\partial x} = P_{yz} + (\mu^s - \sigma_o)\frac{\partial^2 w}{\partial x^2} \\ &= P_{yz} + \frac{\mu^s - \sigma_o}{2}[\Omega''(z) + \overline{\Omega''(z)}]^-\end{aligned} \tag{16b}$$

As a particular case, we consider the situation when the solid is subjected to a uniform remote shear stress $\sigma_{yz}=\sigma^\infty_{yz}$ and a traction-free crack face ($P_{yz}=0$). From Eqs. (9), (16*a*), and (16*b*), the surface condition on either side of the crack can be formulated as follows.

On the upper face,

$$\frac{\mu i}{2}[\Omega'(z) - \overline{\Omega'(z)}]^+ = -\frac{\mu^s - \sigma_o}{2}[\Omega''(z) + \overline{\Omega''(z)}]^+ \tag{17a}$$

On the lower face,

$$\frac{\mu i}{2}[\Omega'(z) - \overline{\Omega'(z)}]^- = \frac{\mu^s - \sigma_o}{2}[\Omega''(z) + \overline{\Omega''(z)}]^- \tag{17b}$$

In antiplane deformations (mode-III crack) it is clear that $w^+=-w^-$, which leads to a Hilbert problem in terms of the derivatives of the unknown function $\Omega(z)$ defined by Eqs. (7), (17*a*), and (17*b*) as follows.

On the upper face,

$$\frac{\mu i}{2}[\Omega'(z) - \overline{\Omega'(z)}]^+ = \frac{\mu^s - \sigma_o}{2}[\Omega''(z) + \overline{\Omega''(z)}]^- \tag{18a}$$

On the lower face,

$$\frac{\mu i}{2}[\Omega'(z) - \overline{\Omega'(z)}]^- = \frac{\mu^s - \sigma_o}{2}[\Omega''(z) + \overline{\Omega''(z)}]^- \tag{18b}$$

Since we have assumed uniform remote stress σ^∞_{yz}, we necessarily have that

$$\Omega'(z) + \overline{\Omega'}(z) = 0, \quad \Omega'(z) = -\overline{\Omega'}(z) \tag{19}$$

In addition, adding Eqs. (18*a*) and (18*b*) yields

$$\begin{aligned}&\frac{\mu i}{2}([\Omega'(z) - \overline{\Omega'}(z)]^+ + [\Omega'(z) - \overline{\Omega'}(z)]^-) \\ &= (\mu^s - \sigma_o)(\Omega''(z)^- + \overline{\Omega''}(z)^+)\end{aligned} \tag{20}$$

Consequently, from Eq. (19), Eq. (20) takes the following form:

$$\mu i(\Omega'(z)^+ + \Omega'(z)^-) = (\mu^s - \sigma_o)(\Omega''(z)^- - \Omega''(z)^+) \tag{21}$$

Next, if we write the unknown $\Omega'(z)$ as a Cauchy integral [19], noting the requirement that the stresses be bounded at the crack tips, we have that

$$\Omega'(z) = \frac{1}{2i\pi}\int_{-a}^{+a}\frac{f(t)}{t-z}dt + \frac{1}{\mu i}[\sigma^\infty_{yz}] \tag{22a}$$

$$\begin{aligned}\Omega''(z) &= \frac{1}{2\pi i}\int_{-a}^{+a}\frac{f(t)dt}{(t-z)^2} = -\left[\frac{f(t)}{t-z}\right]_{-a}^{a} + \frac{1}{2\pi i}\int_{-a}^{+a}\frac{f'(t)dt}{t-z} \\ &= \frac{1}{2\pi i}\int_{-a}^{+a}\frac{f'(t)dt}{t-z}\end{aligned} \tag{22b}$$

where

$$f(t_0) = \Omega'(z)^+ - \Omega'(z)^-, \quad -a \le t_o \le a$$

$$f(a) = f(-a) = 0 \text{ (finite stress at the crack tips)}$$

Finally, from Eqs. (21), (22*a*), and (22*b*), we obtain the following first-order Cauchy singular integro-differential equation for the unknown $f(t)$, $t\in[-a,a]$:

$$\frac{\mu}{\pi}\int_{-a}^{a}\frac{f(t)dt}{t-t_o}+2[\sigma_{yz}^{\infty}]=-(\mu^s-\sigma_o)f'(t_o),\quad -a\le t_o\le a$$

$$f(a)=f(-a)=0 \tag{23}$$

3 Investigation of the Cauchy Singular Integro-Differential Equation

The Cauchy singular integro-differential equation (23) closely resembles the well-known and well-studied classical Prandtl's singular integro-differential from aerodynamics.

$$\frac{\Gamma(x)}{B(x)}-\frac{1}{2\pi}\int_{-1}^{1}\frac{\Gamma'(t)dt}{t-x}=f(x),\quad -1\le x\le 1$$

$$\Gamma(1)=\Gamma(-1)=0$$

where $\Gamma(x)$ is the unknown function and $B(x)$ and $f(x)$ are known functions (see, for example, Ref. [23] and the references therein). Unfortunately, the differences between Eq. (23) and Prandtl's equation are sufficiently significant so that the many existing results on the solution of Prandtl's equation (numerical or otherwise) do not accommodate Eq. (23). In Ref. [24], Frankel discussed a Galerkin approach for solving a class of singular integro-differential equations similar in form to Eq. (23) but appearing in the study of infrared gaseous radiation and molecular conduction as well as in elastic contact studies. Frankel's methods were among the three methods used subsequently in Ref. [20] to find numerical solutions of singular integro-differential equations of the type described by Eq. (23).

In this section, we adapt the collocation methods used in Refs. [23,24] to find numerical solutions of Eq. (23).

3.1 Solution of Singular Integro-Differential Equation by a Collocation Method. Consider Eq. (23),

$$\frac{\mu}{\pi}\int_{-a}^{a}\frac{f(t)dt}{t-t_o}+2[\sigma_{yz}^{\infty}]=-(\mu^s-\sigma_o)\frac{df(t_o)}{dt_o},\quad -a\le t_o\le a$$

$$f(a)=f(-a)=0$$

where

$$f(t_0)=\Omega'(z)^{+}-\Omega'(z)^{-},\quad \Omega'(z)=\frac{1}{2\pi i}\int_{-a}^{a}\frac{f(t)}{t-z}dt+\frac{1}{\mu i}[\sigma_{yz}^{\infty}] \tag{24}$$

Set $t/a=x$ in Eq. (24) and obtain

$$\frac{\mu}{\pi}\int_{-1}^{1}\frac{f(ax)dx}{x-x_o}+2[\sigma_{yz}^{\infty}]=-(\mu^s-\sigma_o)\frac{df(ax_o)}{d(ax_o)},\quad -1\le x_o\le 1 \tag{25}$$

Rewriting $x\to t$, $x_o\to t_o$ and further defining $f(at)=u(t)$, from Eq. (25), we have the following:

$$\frac{(\mu^s-\sigma_o)}{a}\frac{du(t_o)}{dt_o}-\frac{\mu}{\pi}\int_{-1}^{1}\frac{u(t)dt}{t_o-t}=-2[\sigma_{yz}^{\infty}],\quad -1\le t_o\le 1$$

$$u(1)=u(-1)=0 \tag{26}$$

After utilizing the inverse operator T^{-1}, as defined by the relation [20],

$$T^{-1}\psi(x)=\frac{1}{\pi\sqrt{1-x^2}}\int_{-1}^{1}\psi(x)dx-\frac{1}{\pi^2\sqrt{1-x^2}}\int_{-1}^{1}\frac{\sqrt{1-t^2}\psi(t)}{t-x}dt$$

$$x\in(-1,1) \tag{27a}$$

$$T(T^{-1}\psi)=\psi$$

and further defining

$$T(u(x))=\int_{-1}^{1}\frac{u(x)}{x-t}dx=\psi(t) \tag{27b}$$

we have from Eq. (26) that

$$u(t_o)=\frac{1}{\pi\sqrt{1-t_o^2}}\int_{-1}^{1}u(t)dt-\frac{1}{\mu\pi\sqrt{1-t_o^2}}\times\int_{-1}^{1}\frac{\sqrt{1-t^2}}{t-t_o}\left(-2[\sigma_{yz}^{\infty}]-\frac{(\mu^s-\sigma_o)}{a}\frac{du(t)}{dt}\right)dt$$

$$t_o\in(-1,1),\quad u(1)=u(-1)=0 \tag{28}$$

Multiplying by $\sqrt{1-t_o^2}$ both sides of Eq. (28) yields

$$u(t_o)\sqrt{1-t_o^2}-\frac{1}{\pi}\int_{-1}^{1}u(t)dt-\left(\frac{\mu^s-\sigma_o}{a\mu\pi}\right)\int_{-1}^{1}\frac{\sqrt{1-t^2}}{t-t_o}\frac{du(t)}{dt}dt=\frac{2[\sigma_{yz}^{\infty}]}{\mu\pi}\int_{-1}^{1}\frac{\sqrt{1-t^2}}{t-t_o}dt \tag{29}$$

Assume that the function $u(t_o)$ has an expansion of the form,

$$u(t_o)=\sum_{m=0}^{N}a_mT_m(t_o),\quad t_o\in[-1,1],\quad m=0,1,2,\ldots \tag{30}$$

where $T_m(t_o)$ represents the mth Chebychev polynomial of the first kind. By imposing end conditions $u(-1)=u(1)=0$ (see Eq. (26)), we find that

$$u(-1)=\sum_{m=0}^{N}a_mT_m(-1)=\sum_{m=0}^{N}a_m(-1)^m=0 \tag{31a}$$

$$u(1)=\sum_{m=0}^{N}a_mT_m(1)=\sum_{m=0}^{N}a_m=0,\quad m=0,1,2,\ldots$$

$$\because T_m(-1)=(-1)^m,\quad T_m(1)=1 \tag{31b}$$

Furthermore,

$$\frac{dT_m(x)}{dx}=mU_{m-1}(x) \tag{32}$$

Here $U_m(x)$ denotes the mth Chebychev polynomial of the second kind. Thus, from Eqs. (30) and (32), we find that

$$\frac{du(t_o)}{dt_o}=\frac{d}{dt_o}\left(\sum_{m=0}^{N}a_mT_m(t_o)\right)=\sum_{m=0}^{N}ma_mU_{m-1}(t_o),\quad t_o\in[-1,1]$$

$$m=0,1,2,\ldots \tag{33}$$

Next, using Eqs. (30) and (33) in Eq. (29) yields

$$\sum_{m=0}^{N}\left[a_mT_m(t_o)\sqrt{1-t_o^2}-\frac{1}{\pi}\int_{-1}^{1}a_mT_m(t)dt-\left(\frac{\mu^s-\sigma_o}{a\mu\pi}\right)\int_{-1}^{1}\frac{\sqrt{1-t^2}}{t-t_o}ma_mU_{m-1}(t)dt\right]=\frac{2[\sigma_{yz}^{\infty}]}{\mu\pi}\int_{-1}^{1}\frac{\sqrt{1-t^2}}{t-t_o}dt,\quad t_o\in(-1,1),\quad m=0,1,2,\ldots \tag{34}$$

In addition, the following properties of the Chebychev polynomials:

$$\text{orthogonality: } \int_{-1}^{1} \frac{T_m(x)T_n(x)}{\sqrt{1-x^2}}dx = \begin{Bmatrix} 0, & m \neq n \\ \pi, & m = n = 0 \\ \frac{\pi}{2}, & m = n > 0 \end{Bmatrix} \tag{35}$$

$$\text{closed-form integral relations: } \int_{-1}^{1} \frac{U_n(t)\sqrt{1-t^2}}{t-x}dt = -\pi T_{n+1}(x), \quad n = 0,1,\ldots \tag{36a}$$

$$\int_{-1}^{1} T_m(x)dx = \frac{1+(-1)^m}{1-m^2}, \quad m = 0,1,2,\ldots \tag{36b}$$

Consequently, by utilizing Eqs. (36*a*) and (36*b*), Eq. (34) reduces to

$$\sum_{m=0}^{N}\left[a_m T_m(t_o)\sqrt{1-t_o^2} - \frac{a_m}{\pi}\left(\frac{1+(-1)^m}{1-m^2}\right) + \left(\frac{\mu^s-\sigma_o}{a\mu}\right)m a_m T_m(t_o)\right] = -\frac{2[\sigma_{yz}^{\infty}]}{\mu}T_1(t_o)$$

We now select the set of collocation points as given by $t_o = t_{oi} = -\cos\left(\frac{i\pi}{N}\right)$ for $i = 1,2,\ldots,N-1$ and thus derive the following system of linear equations:

$$\sum_{m=0}^{N} a_m\left[T_m(t_{oi})\sqrt{1-t_{oi}^2} - \frac{1}{\pi}\left(\frac{1+(-1)^m}{1-m^2}\right) + \left(\frac{\mu^s-\sigma_o}{a\mu}\right)m T_m(t_{oi})\right] = -\frac{2[\sigma_{yz}^{\infty}]}{\mu}T_1(t_{oi}), \quad i = 1,2,\ldots,N-1 \tag{37}$$

Noting the following property of the Chebychev polynomials of the first kind $T_n(\cos\theta) = \cos(n\theta)$, Eq. (37) further reduces to the following compact form:

$$\sum_{m=0}^{N} a_m\left[-\cos\left(\frac{mi\pi}{N}\right)\sqrt{1-\left(\cos\left(\frac{i\pi}{N}\right)\right)^2} - \frac{1+(-1)^m}{\pi(1-m^2)} - mS_e\cos\left(\frac{mi\pi}{N}\right)\right] = 2S\cos\left(\frac{i\pi}{N}\right), \quad \text{for } 1 \le i \le N-1 \tag{38}$$

where

$$S_e = \frac{\mu^s-\sigma_o}{a\mu}(\text{surface stress})$$

and

$$S = \frac{[\sigma_{yz}^{\infty}]}{\mu}(\text{remote stress})$$

In addition, from the end condition equations (31*a*) and (31*b*), we have that

$$\sum_{m=0}^{N} a_m(1)^m = 0 \quad \text{for } i = 0, \quad \sum_{m=0}^{N} a_m(-1)^m = 0, \quad i = N$$

$$i = 0,1,2,\ldots \tag{39}$$

The solution of Eq. (24) is now reduced to the solution of the system of equations (38) and (39) for the constant a_m. The latter can be achieved using any of the existing commercial numerical software packages (e.g., MATLAB, MAPLE, NAG, etc.) and is the subject of Sec. 4.

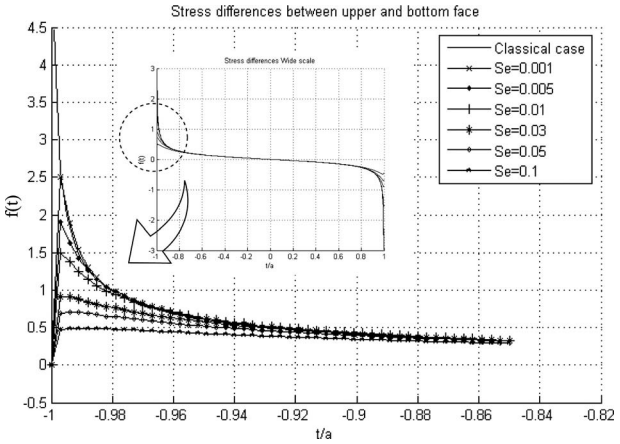

Fig. 2 Stress differences between the upper and bottom faces where $\sigma_{yz}^{\infty}/\mu = 0.1$

4 Results and Discussion

In this section, the numerical solution of Eqs. (38) and (39) is performed for a range of surface parameters obtained from the work of Sharma and Ganti in Ref. [10]. It is found that the numerical method performs well for problems of this type guaranteeing rapid convergence (see, for example, Fig. 2).

$$S_e: 0.1 < S_e < 0.001$$
$$\mu^s = 161.73 \ (\text{J/m}^2), \quad \sigma_o = 1.3 \ (\text{J/m}^2), \quad \mu = 168 \ (\text{GPa}) \tag{40}$$

4.1 Comparison With Known Classical Results. To verify the mathematical model, we first reproduce, as a special case of our analysis, the solution of the classical antiplane crack problem in which surface effects are neglected. The latter problem has corresponding analytic solutions described by Refs. [19,21,22].

$$\Omega'(z) = \frac{1}{\mu}[\sigma_{xz} - i\sigma_{yz}] = \frac{-i\sigma_{yz}^{\infty}z}{\mu\sqrt{z^2-a^2}}$$

Evaluating $\Omega'(z)(-a < t < a)$, we have the following.

On the upper face,

$$\Omega'(z)^+ = \frac{-i\sigma_{yz}^{\infty}t}{\mu\sqrt{-(a^2-t^2)}} = \frac{-i\sigma_{yz}^{\infty}t}{\mu i\sqrt{(a^2-t^2)}} = \frac{-\sigma_{yz}^{\infty}t}{\mu\sqrt{a^2-t^2}} \tag{41a}$$

On the lower face,

$$\Omega'(z)^- = \frac{i\sigma_{yz}^{\infty}t}{\mu\sqrt{-(a^2-t^2)}} = \frac{i\sigma_{yz}^{\infty}t}{\mu i\sqrt{(a^2-t^2)}} = \frac{\sigma_{yz}^{\infty}t}{\mu\sqrt{a^2-t^2}} \tag{41b}$$

(We note here that from Eq. (8), σ_{yz} is zero yet σ_{xz} is nonzero). Then the stress difference between the upper and lower faces can be defined from Eqs. (41*a*) and (41*b*) by

$$\Omega'(z)^+ - \Omega'(z)^- = \frac{-2\sigma_{yz}^{\infty}t}{\mu\sqrt{a^2-t^2}}, \quad -a < t < a \tag{42}$$

Returning to our formulation, the corresponding stress differences are defined in terms of the function $f(t)$ by (see Eq. (24))

$$\Omega'(z)^+ - \Omega'(z)^- = f(t) \tag{43}$$

The values of $f(t)$ are plotted in Fig. 2, where the parameter S_e is varied by changing the dimension of the crack (i.e., 10 nm $< a <$ 1 μm).

It is clear from Fig. 2 that as the surface effect becomes negli-

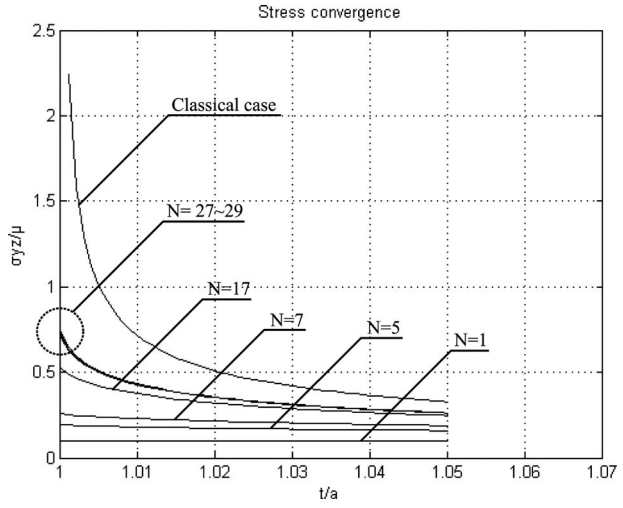

Fig. 3 Stress convergence versus the number of iterations (*N*)

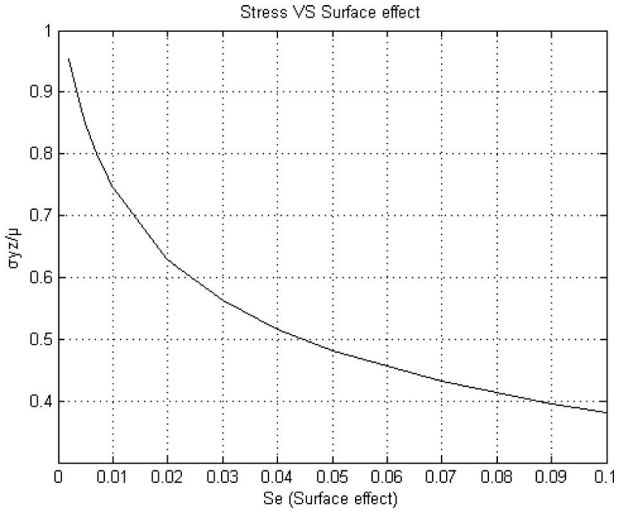

Fig. 5 Stress (at the crack tip) versus surface effect when $\sigma_{yz}^{\infty}/\mu=0.1$

gible, our solution reduces to that of the classical case, even at the crack tip where the stress difference becomes infinite.

4.2 Stress Distributions at the Crack Tip. Based on the numerical solution of $f(t)$ derived in Sec. 4.1, the corresponding stress distributions can be found from Eq. (22*a*).

$$\Omega'(z)=\frac{1}{2i\pi}\int_{-a}^{+a}\frac{f(t)}{t-z}dt+\frac{1}{\mu i}[\sigma_{yz}^{\infty}]$$

These results are presented in Figs. 3 and 4. In fact, Fig. 3 clearly illustrates rapid convergence of the method (in approximately 30 iterations) but more importantly, it is clear that, in contrast to the classical case (where surface effects are neglected), the stresses at the crack tip *remain finite*.

Furthermore, from Fig. 4 we see that stresses relatively far from the crack tips converge to the value 0.1, which is the magnitude of the applied remote stress. These results agree with the well-known results from classical elasticity (that the effect of stress concentration and surface stress/energy is localized).

Finally, Fig. 5 demonstrates the relation between stress (at the crack tip) and the surface effect. It is clear that stress at the crack tip increases when the surface effect becomes negligible (as predicted by the corresponding classical problem where surface effects are neglected). Furthermore, since the surface parameter S_e is controlled by variations in the crack length, our results also indicate that the corresponding stresses are strongly dependent on crack size.

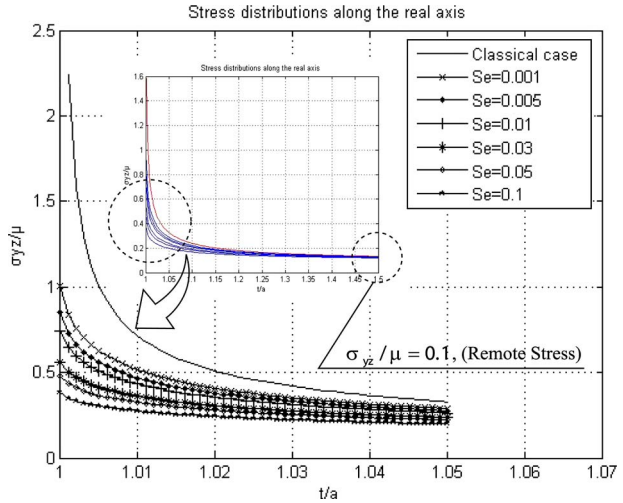

Fig. 4 Stress distribution with respect to surface parameter (S_e) when $\sigma_{yz}^{\infty}/\mu=0.1$

5 Conclusions

In this paper, we have examined the effects of surface elasticity in a classical mode-III crack problem arising in the antiplane shear deformations of a linearly elastic solid. The surface mechanics are incorporated using the continuum based surface/interface model of Gurtin and Murdoch. Complex variable methods are used to obtain an exact complete solution (not simply a crack tip solution) by reducing the problem to a Cauchy singular integro-differential equation of the first order. Finally, classical collocation methods are adapted to obtain numerical solutions, which demonstrate several interesting phenomena in the case when the solid incorporates a traction-free crack face and is subjected to uniform remote loading. In particular, we note that, in contrast to the classical result from linear elastic fracture mechanics, the stresses at the (sharp) crack tip remain finite. The techniques used here are sufficiently general to accommodate the analogous problems from plane elasticity. This will be the subject of a future paper.

Acknowledgment

This work was supported by the Natural Sciences and Engineering Research Council of Canada through Grant No. NSERC OGP 115112. The authors would like to acknowledge the numerous useful discussions with Jay Frankel and Paul Martin.

References

[1] Buehler, M. J., and Gao, H. J., 2006, "Dynamical Fracture Instabilities Due to Local Hyperelasticity at Crack Tips," Nature (London), **439**, pp. 307–310.
[2] Buehler, M. J., Abraham, F. F., and Gao, H. J., 2003, "Hyperelasticity Governs Dynamic Fracture at a Critical Length Scale," Nature (London), **426**, pp. 141–146.
[3] Buehler, M. J., Gao, H. J., and Huang, Y. G., 2004, "Continuum and Atomistic Studies of the Near-Crack Field of a Rapidly Propagating Crack in a Harmonic Lattice," Theor. Appl. Fract. Mech., **41**, pp. 21–42.
[4] Abraham, F. F., Broughton, J. Q., Bernstein, N., and Kaxiras, E., 1998, "Spanning the Continuum to Quantum Length Scales in a Dynamic Simulation of Brittle Fracture," Europhys. Lett., **44**, pp. 783–787.
[5] Miller, R. E., and Shenoy, V. B., 2000, "Size-Dependent Elastic Properties of Nanosized Structural Elements," Nanotechnology, **11**, pp. 139–147.
[6] Shenoy, V. B., 2002, "Size-Dependent Rigidities of Nanosized Torsional Elements," Int. J. Solids Struct., **39**, pp. 4039–4052.
[7] Gurtin, M. E., and Murdoch, A. I., 1975, "A Continuum Theory of Elastic Material Surfaces," Arch. Ration. Mech. Anal., **57**(4), pp. 291–323.
[8] Gurtin, M. E., Weissmuller, J., and Larche, F., 1998, "A General Theory of

Curved Deformable Interface in Solids at Equilibrium," Philos. Mag. A, **78**(5), pp. 1093–1109.
[9] Tian, L., and Rajapakse, R. K. N. D., 2007, "Analytical Solution of Size-Dependent Elastic Field of a Nano-Scale Circular Inhomogeneity," ASME J. Appl. Mech., **74**(3), pp. 568–574.
[10] Sharma, P., and Ganti, S., 2004, "Size-Dependent Eshelby's Tensor for Embedded Nano-Inclusions Incorporating Surface/Interface Energies," ASME J. Appl. Mech., **71**(5), pp. 663–671.
[11] Duan, H. L., Wang, J., Huang, Z. P., and Karhaloo, B. L., 2005, "Size-Dependent Effective Elastic Constants of Solids Containing Nano-Inhomogeneities With Interface Stress," J. Mech. Phys. Solids, **53**(7), pp. 1574–1596.
[12] Cammarata, R. C., 1997, "Surface and Interface Stress Effects on Interfacial and Nanostructured Materials," Mater. Sci. Eng., A, **237**(2), pp. 180–184.
[13] Hoagland, R. G., Daw, M. S., and Hirth, J. P., 1991, "Some Aspects of Forces and Fields in Atomic Models of Crack Tips," J. Mater. Res., **6**, pp. 2565–2571.
[14] Wang, G.-F., Feng, X.-Q., Wang, T.-J., and Gao, W., 2008, "Surface Effects on the Near-Tip Stresses for Mode-I and Mode-III Cracks," ASME J. Appl. Mech., **75**, pp. 1–5.
[15] Gill, S. P. A., 2007, "The Effect of Surface-Stress on the Concentration of Stress at Nanoscale Surface Flaws," Int. J. Solids Struct., **44**, pp. 7500–7509.
[16] Wu, C. H., 1999, "The Effect of Surface Stress on the Configurational Equilibrium of Voids and Cracks," J. Mech. Phys. Solids, **47**, pp. 2469–2492.
[17] Wu, C. H., and Wang, M. L., 2000, "The Effect of Crack-Tip Point Loads on Fracture," J. Mech. Phys. Solids, **48**, pp. 2283–2296.
[18] Wu, C. H., and Wang, M. L., 2001, "Configurational Equilibrium of Circular-Arc Cracks With Surface Stress," Int. J. Solids Struct., **38**, pp. 4279–4292.
[19] Muskhelishvili, N. I., 1953, *Some Basic Problems of the Mathematical Theory of Elasticity*, Noordhoff, Groningen, The Netherlands.
[20] Chakrabarti, A., and Hamsapriye, 1999, "Numerical Solution of a Singular Integro-Differential Equation," ZAMM, **79**(4), 233–241.
[21] England, A. H., 1971, *Complex Variable Methods in Elasticity*, Wiley, London.
[22] Sih, G. C., 1965, "Boundary Problems for Longitudinal Shear Cracks," Dev. Theor. Appl. Mech., **2**, pp. 117–130.
[23] Ioakimidis, N. I., 1984, "A Natural Interpolation Formula for Prandtl's Singular Integrodifferential Equation," Int. J. Numer. Methods Fluids, **4**, pp. 283–290.
[24] Frankel, J. I., 1995, "A Galerkin Solution to a Regularized Cauchy Singular Integro-Differential Equation," Q. Appl. Math., **LIII**(2), pp. 245–258.